Tunable momentum pair creation of spin excitations in dipolar bilayers

Thomas Bilitewski,[1] G. A. Domínguez-Castro,[2] David Wellnitz,[3,4] Ana Maria Rey,[3,4] and Luis Santos[2]

[1]*Department of Physics, Oklahoma State University, Stillwater, Oklahoma 74078, USA*

[2]*Institut für Theoretische Physik, Leibniz Universität Hannover, Appelstrasse 2, D-30167 Hanover, Germany*

[3]*JILA, National Institute of Standards and Technology and Department of Physics, University of Colorado, Boulder, Colorado 80309, USA*

[4]*Center for Theory of Quantum Matter, University of Colorado, Boulder, Colorado 80309, USA*

(Received 20 February 2023; revised 19 May 2023; accepted 10 July 2023; published 19 July 2023)

We study the temporal growth and spatial propagation of quantum correlations in a two-dimensional bilayer realizing a spin-1/2 quantum *XXZ* model with couplings mediated by long-range and anisotropic dipolar interactions. Starting with an initial state consisting of spins with opposite magnetization in each of the layers, we predict a dynamic instability that results, at short times, in the creation of correlated pairs of excitations at specific momenta at exponentially fast rates and entanglement between spatially separated modes. The momentum structure of the created pairs can be controlled via the dipolar orientation, the layer separation, or the dipolar couplings. The predicted behavior remains observable at very low filling fractions, making it accessible in state-of-the-art experiments with Rydberg atoms, magnetic atoms, and polar molecule arrays.

DOI: 10.1103/PhysRevA.108.013313

I. INTRODUCTION

Anisotropic dipolar interactions controllable via electromagnetic fields offer unique opportunities for the implementation of iconic models of quantum magnetism relevant for fundamental science and for the development of novel quantum technologies. In recent years, great progress has been made on the implementation of dipole-induced spin-exchange interactions in fully controllable quantum systems of polar molecules [1–3], magnetic atoms [4], and Rydberg atoms [5,6]. However, most of the investigations so far have been targeted to the single-excitation regime [7] or to the case of multiple excitations characterized via collective observables [8–17]. Nevertheless, recent experimental developments on quantum gas microscopes [18,19] and optical tweezers [20–24] that allow for the spatially resolved control of correlations at the single-particle level are opening a window to explore rich and intriguing quantum phenomena enabled by dipolar spin models.

In this work, we study the temporal and spatial growth of correlations during the many-body dynamics of an array of spin-1/2 frozen dipoles confined in two separated two-dimensional layers [see Fig. 1(a)]. This system, implementable, for example, using optical lattices or tweezer arrays, realizes a quantum *XXZ* spin model with dipolar couplings. By preparing the two layers in opposite spin states, as in recent experiments on polar molecules [15], one creates a dynamically unstable state from which correlated pairs of spin excitations develop and grow at an exponential rate, at least at short times. These correlated pairs manifest in the spin structure factor, which develops intriguing momentum patterns controllable by both the separation of the layers and the magnitude and orientation of the dipole moments.

The buildup of spin correlations can be explained using a Bogoliubov analysis, which uncovers a dynamical instability in specific tunable momentum modes. We validate the Bogoliubov predictions of the pair creation patterns by numerical simulations of the full spin dynamics and show that pattern formation remains robust even for very low lattice fillings, making it observable in state-of-the-art experiments, without requiring unit filling.

Here we find the exponential proliferation of correlated pairs of excitations in spatially separated layers. This emulates the phenomenon of pair creation from vacuum fluctuations, opening unique opportunities for quantum simulation and for fundamental tests of quantum mechanics including Einstein-Podolsky-Rosen (EPR) steering [25–28]. Pair creation itself is a ubiquitous phenomenon in physics, relevant in a broad range of contexts including parametric amplification and two-mode squeezing in quantum optics [29], the Schwinger effect in high-energy physics [30–32], the emission of Unruh thermal radiation in curved space time [33,34], and in holography given that the thermofield double state generated during pair production is dual to a traversable wormhole [35,36] in quantum gravity, and a resource for quantum teleportation [37–39].

Previous studies of pair creation processes in spinor condensates induced by contact interactions [40–43] were dominated by single (resonant) momentum modes (or trap states in confined condensates [44]) determined by the quadratic Zeeman shift, while proposals of pair production in cavities induced by collective interactions [45] require a set of laser tones to generate nontrivial patterns and are sensitive to cavity loss [46]. In contrast, the pair creation observed in this work allows for the generation of highly tunable and intriguing distributions of excitations naturally emerging from anisotropic dipolar couplings [1–4,8–11,13,47,48].

II. MODEL

We consider an array of frozen dipoles with two relevant internal levels (e.g., two rotational states in the case of polar

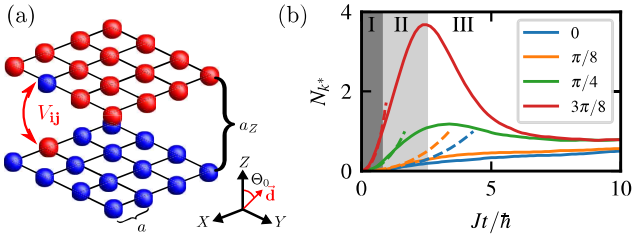

FIG. 1. System. (a) Bilayer of dipoles confined in two-dimensional (2D) planes with dipole moments aligned at an angle Θ_0 to the out-of-plane direction. When the layers are prepared in an initial state with opposite magnetization, dipolar interlayer interactions create pairs of excitations in the layers in specific quasimomentum modes. (b) Occupation of the most unstable mode N_{k^*} as a function of time t for different dipole orientations Θ_0 (legend) at fixed $a_Z/a = 2$. Shown are spin dynamics from DTWA (solid lines) and the prediction from Bogoliubov theory (dashed lines). Shaded regions indicate the regimes of dynamics (for $\Theta_0 = 3\pi/8$), where we find exponential growth as predicted by Bogoliubov (I), saturation and slow down of growth (II), and eventual decay and thermalization (III). Results are for a 33×33 bilayer at unit filling.

molecules) confined in two parallel two-dimensional layers generated via optical lattices or optical tweezers, separated by a tunable distance a_Z. We denote the upper layer as A and the lower one as B. As shown in Fig. 1(a), both layers have square geometry with a nearest-neighbor spacing a.

Electric and magnetic dipole-dipole interactions can lead to both exchange of internal-state excitations as well as Ising interactions [7–13,47,49], which can be tuned via external electromagnetic fields. For the case of frozen particles, the dynamics is governed by the celebrated (long-range) spin-1/2 *XXZ* model,

$$\hat{H}_{XXZ} = \frac{1}{2}\sum_{\sigma=A,B}\sum_{\mathbf{i}\neq\mathbf{j}} V_{\mathbf{ij}}^{\sigma\sigma}\left(\hat{s}_{\mathbf{i}\sigma}^{+}\hat{s}_{\mathbf{j}\sigma}^{-} + \hat{s}_{\mathbf{i}\sigma}^{-}\hat{s}_{\mathbf{j}\sigma}^{+} + 2\eta\hat{s}_{\mathbf{i}\sigma}^{z}\hat{s}_{\mathbf{j}\sigma}^{z}\right) + \sum_{\mathbf{i},\mathbf{j}} V_{\mathbf{ij}}^{AB}\left(\hat{s}_{\mathbf{i}A}^{+}\hat{s}_{\mathbf{j}B}^{-} + \hat{s}_{\mathbf{i}A}^{-}\hat{s}_{\mathbf{j}B}^{+} + 2\eta\hat{s}_{\mathbf{i}A}^{z}\hat{s}_{\mathbf{j}B}^{z}\right), \quad (1)$$

where σ indexes the layers, η characterizes the relative strength between Ising and exchange couplings, and $\mathbf{i} = (i_x, i_y)$ stands for a two-dimensional coordinate in which i_x, i_y run along the positions in a given two-dimensional layer of size $N = L \times L$. As is customary, the spin operators $\hat{s}_{\mathbf{i}}^{\alpha} = \hat{\sigma}_{\mathbf{i}}^{\alpha}/2$ are given in terms of the Pauli matrices $\hat{\sigma}^{x,y,z}$ that act on the spin at site $\mathbf{i}$. We shall focus our attention on dipole couplings of the form

$$V_{\mathbf{ij}}^{\sigma\sigma'} = \frac{J}{\left|\mathbf{r}_{\mathbf{i}}^{\sigma} - \mathbf{r}_{\mathbf{j}}^{\sigma'}\right|^3}\left\{1 - \frac{3\left[\mathbf{d}\cdot\left(\mathbf{r}_{\mathbf{i}}^{\sigma} - \mathbf{r}_{\mathbf{j}}^{\sigma'}\right)\right]^2}{\left|\mathbf{r}_{\mathbf{i}}^{\sigma} - \mathbf{r}_{\mathbf{j}}^{\sigma'}\right|^2}\right\}, \quad (2)$$

where $\hat{\mathbf{d}} = \sin\Theta_0\hat{e}_x + \cos\Theta_0\hat{e}_z$ is the orientation of the dipoles, $\mathbf{r}_{\mathbf{i}}^{\sigma}$ is the position of a dipole in layer σ, and J is the spin-exchange constant.

Motivated by recent experiments on polar molecules in bilayers [15], we consider in the following the nonequilibrium dynamics of this system starting from an initial state where all dipoles in layer A (B) are initially in the spin-up (-down) state. We first analyze the spin excitations in terms of a Bogoliubov treatment, and then by simulating the quantum dynamics of the full dipolar spin model using the discrete truncated Wigner approximation (DTWA) [50,51].

III. BOGOLIUBOV ANALYSIS

As in the standard spin-wave analysis, the spin dynamics can be described by mapping the Hamiltonian (1) to a hard-core bosonic model using the Holstein-Primakoff transformation $\hat{s}_{A,\mathbf{i}}^{z} = 1/2 - \hat{a}_{\mathbf{i}}^{\dagger}\hat{a}_{\mathbf{i}}$, $\hat{s}_{A,\mathbf{i}}^{+} = \hat{a}_{\mathbf{i}}$, $\hat{s}_{A,\mathbf{i}}^{-} = \hat{a}_{\mathbf{i}}^{\dagger}$, and $\hat{s}_{B,\mathbf{i}}^{z} = -1/2 + \hat{b}_{\mathbf{i}}^{\dagger}\hat{b}_{\mathbf{i}}$, $\hat{s}_{B,\mathbf{i}}^{+} = \hat{b}_{\mathbf{i}}^{\dagger}$, $\hat{s}_{B,\mathbf{i}}^{-} = \hat{b}_{\mathbf{i}}$. The bosonic operators $\hat{a}_{\mathbf{i}}$ and $\hat{b}_{\mathbf{i}}$ characterize the spin excitations that appear on top of the prepared initial state.

Assuming a small population of spin excitations, much smaller than the number of sites, the Hamiltonian may be rewritten in quasimomentum space,

$$\hat{H} = \sum_{\mathbf{k}} \tilde{\varepsilon}_{\mathbf{k}}(\hat{a}_{\mathbf{k}}^{\dagger}\hat{a}_{\mathbf{k}} + \hat{b}_{\mathbf{k}}^{\dagger}\hat{b}_{\mathbf{k}}) + \Omega_{\mathbf{k}}\hat{a}_{\mathbf{k}}^{\dagger}\hat{b}_{-\mathbf{k}}^{\dagger} + \Omega_{\mathbf{k}}^{*}\hat{b}_{-\mathbf{k}}\hat{a}_{\mathbf{k}}, \quad (3)$$

where $\hat{a}_{\mathbf{k}} = \frac{1}{\sqrt{N}}\sum_{\mathbf{r}_{\mathbf{i}}} e^{-i\mathbf{k}\cdot\mathbf{r}_{\mathbf{i}}}\hat{a}_{\mathbf{i}}$ and $\hat{b}_{\mathbf{k}} = \frac{1}{\sqrt{N}}\sum_{\mathbf{r}_{\mathbf{i}}} e^{-i\mathbf{k}\cdot\mathbf{r}_{\mathbf{i}}}\hat{b}_{\mathbf{i}}$. The momentum-dependent interlayer coupling is given by $\Omega_{\mathbf{k}} = \sum_{\mathbf{j}} V_{0\mathbf{j}}^{AB} e^{-i\mathbf{k}\cdot\mathbf{r}_{\mathbf{j}}}$, whereas the intralayer band dispersion for spin excitations in each layer is $\tilde{\varepsilon}_{\mathbf{k}} = \varepsilon_{\mathbf{k}} - \eta(\varepsilon_0 - \Omega_0)$, with $\varepsilon_{\mathbf{k}} = \sum_{\mathbf{j}\neq 0} V_{0\mathbf{j}}^{AA} e^{-i\mathbf{k}\cdot\mathbf{r}_{\mathbf{j}}}$. The Ising term results in a momentum-independent shift of the intralayer band energy. The interlayer coupling drives the creation of correlated pairs of excitations (one per layer) at an energy cost set by the intralayer term.

The Hamiltonian can be diagonalized by means of a Bogoliubov transformation (see the Appendix), which leads to the eigenenergies $\xi_{\mathbf{k}} = \sqrt{\tilde{\varepsilon}_{\mathbf{k}}^2 - |\Omega_{\mathbf{k}}|^2}$. Crucially, $|\Omega_{\mathbf{k}_c}| > |\tilde{\varepsilon}_{\mathbf{k}_c}|$ for certain quasimomenta $\mathbf{k}_c$, resulting in imaginary eigenenergies $\xi_{\mathbf{k}_c}$, i.e., a dynamical instability of the vacuum of spin excitations leading to the creation of correlated pairs. The instability manifests itself as an exponential growth in the population of the corresponding mode, $N_{\mathbf{k}_c} = (|\Omega_{k_c}|/|\xi_{\mathbf{k}_c}|)^2 \sinh^2(|\xi_{\mathbf{k}_c}|t)$. These predictions are shown as the dashed lines in Fig. 1(b), compared to the full spin dynamics discussed below.

Note that if $a_Z^3 \gg a^3$, the interlayer coupling $|\Omega_{\mathbf{k}}|$ is much smaller than the intralayer bandwidth. As a result, imaginary eigenenergies only occur for $\tilde{\varepsilon}_{\mathbf{k}} \simeq 0$. This condition is modified by the shift induced by the Ising term, which hence acts as an additional knob to tailor the quasimomentum distributions discussed below [a similar control knob would be provided by a layer bias of the form $\sum_i(\hat{s}_{A,\mathbf{i}}^{z} - \hat{s}_{B,\mathbf{i}}^{z})$] (see the Appendix). In the following, we mostly focus, for simplicity, on the case $\eta = 0$, i.e., in the absence of the Ising term (*XY* model), for which $\tilde{\varepsilon}_{\mathbf{k}} = \varepsilon_{\mathbf{k}}$.

Figure 2(a) shows the pair coupling strength $\Omega_{\mathbf{k}}$ in the Brillouin zone, overlaid with the resonant line for which $\varepsilon_{\mathbf{k}} \simeq 0$. Pairs are most effectively produced exactly on resonance and for momenta where pair coupling is strong. This is borne out in Fig. 2(b), which shows the growth rate of momentum modes, i.e., the imaginary part of the Bogoliubov energy, which matches with the overlap of the resonant surface and the region of strong interlayer coupling seen in Fig. 2(a). Bogoliubov theory hence predicts the creation of pairs with a specific quasimomentum distribution. Figure 2(c) shows the growth rate Γ of the most unstable mode, i.e., the maximum of

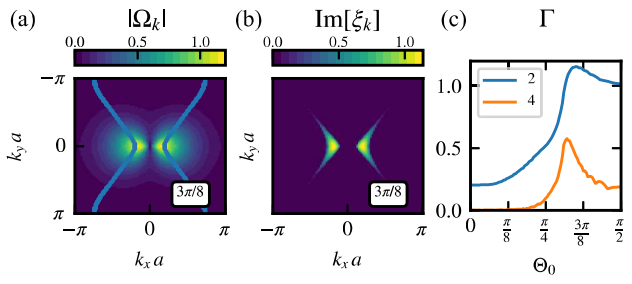

FIG. 2. Bogoliubov analysis. (a) Pair coupling strength $|\Omega_k|$ as a color plot, overlaid with the resonant surface $\varepsilon(k) \simeq 0$. (b) Imaginary part of the Bogoliubov energy ξ_k. Both are for a dipole orientation $\Theta_0 = 3\pi/8$ and $a_Z/a = 2$. (c) Growth rate of the maximally unstable mode $\Gamma = \max_k \mathrm{Im}[\xi_k]$ as a function of the dipole orientation Θ_0 at $a_Z/a = 2, 4$ as indicated in the legend. All are in units of $J/\hbar$.

the imaginary part of the Bogoliubov energies, as a function of the dipole orientation Θ_0 for two different bilayer spacings a_Z. At sufficiently long times, the most unstable modes eventually dominate pair creation, resulting in vastly different dynamical scales for the spin excitations for different dipole orientations. Since the overall form of the growth rate does not qualitatively change for $a_Z^3 \gg a^3$, we will focus on the case $a_Z/a = 2$.

IV. TUNABILITY AND CONTROL OVER UNSTABLE MODES

Next we illustrate the tunability of and control over the momentum structure of the dynamical instability, which controls the spatial structure of the created pair correlations and entanglement, and the growth rate of the most unstable modes, as well as the topology of the unstable modes. In particular, we demonstrate how the topology changes from a simply connected circular manifold at $\Theta_0 = 0$ to two disconnected arcs above a critical Θ_0.

There are different natural parameters that allow us to tune the pair creation instabilities. They are the orientation of the dipoles Θ_0 via the field direction, or a shift of the intralayer dispersion $\tilde{\varepsilon}_{\mathbf{k}}$, which may be induced either by an Ising term $\hat{s}_i^z \hat{s}_j^z$ in the dipolar interactions present at finite electric fields or by a layer bias of the form $h \sum_i (\hat{s}_{A,\mathbf{i}}^z - \hat{s}_{B,\mathbf{i}}^z)$ induced by an electric field gradient.

We begin by illustrating the effect of changing the dipole orientation in Fig. 3. We note that the intralayer dispersion (top row) shows a Dirac conelike structure at $\Theta_0 = 0$, with linear scaling around $k = 0$ with an almost rotationally symmetric dispersion, whereas at any finite Θ_0 the dispersion becomes strongly anisotropic. Similar behavior is seen in the interlayer coupling $\Omega_{\mathbf{k}}$ in the middle row. We also note that for the chosen layer spacing $a_Z/a = 2$, the intralayer dispersion is significantly larger than the pair coupling. Since the Bogoliubov dispersions (bottom row) are given by $\xi_{\mathbf{k}} = \sqrt{\tilde{\varepsilon}_{\mathbf{k}}^2 - |\Omega_{\mathbf{k}}|^2}$, we find unstable modes with zero real part close to regions of vanishing dispersion only. We also emphasize that the unstable modes form a ringlike structure for $\Theta_0 = 0$, whereas the unstable modes form two separate arclike features for the other orientations.

We separately illustrate the full tunability of the manifolds of unstable modes through distinct topologies via the dipole orientation in Fig. 4. We observe both a change from a connected circular structure to separate arcs, as well as a

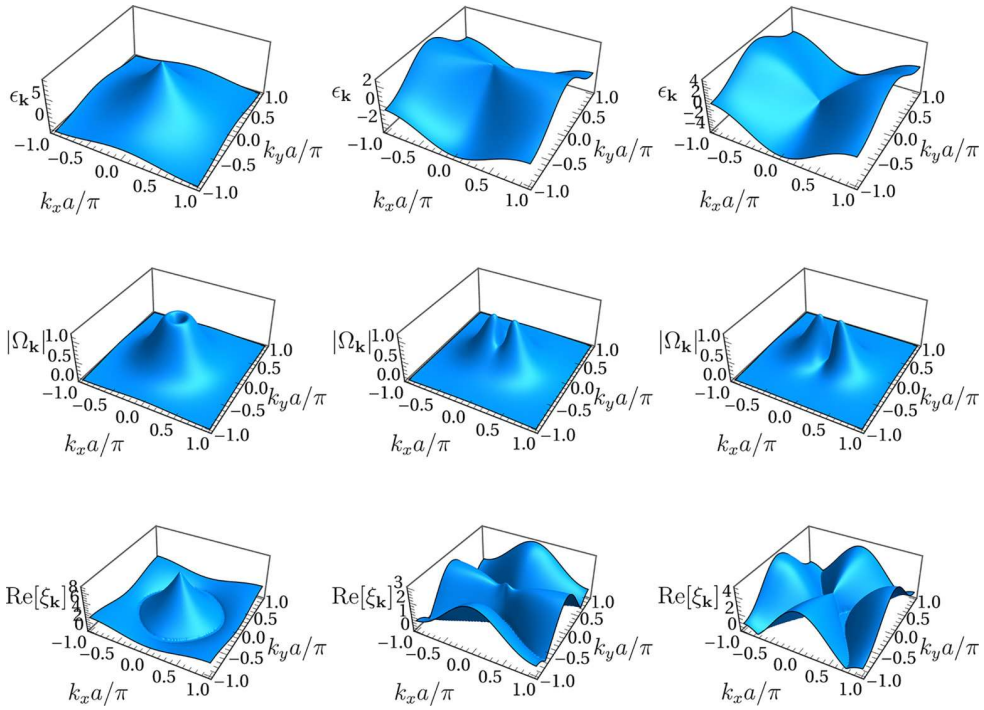

FIG. 3. Tunability of quasiparticle dispersions via electric field orientation. Intraplane dispersion $\varepsilon_{\mathbf{k}}$ (top row), interlayer coupling $\Omega_{\mathbf{k}}$ (middle row), and real part of Bogoliubov energy $\xi_{\mathbf{k}}$ (bottom row), all in units of $J/\hbar$ for different dipole orientations $\Theta_0 = 0, \pi/4, 3\pi/8$ (left to right columns) at a layer separation of $a_Z/a = 2$.

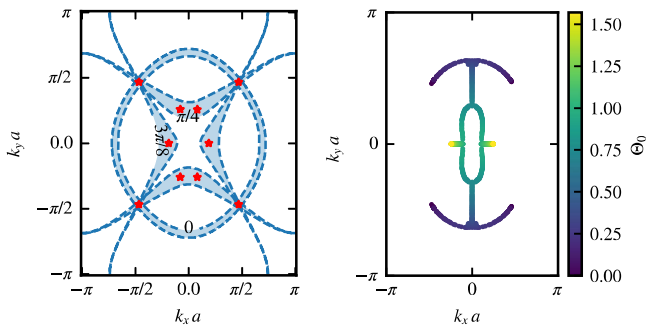

FIG. 4. Tunability of unstable modes via electric field orientation. Left panel: Manifolds of unstable modes defined as the nonvanishing imaginary part of the Bogoliubov energy $\xi_{\mathbf{k}}$. Red stars indicate the most unstable mode. Right panel: Contours of most unstable mode $\mathbf{k}_*$ as a function of dipole orientation Θ_0 (color bar).

change in the number of most unstable modes, from 2 to 4, for different dipole orientations.

In addition, we may also tune the instability by a shift of the dispersion. For simplicity, we consider an applied electric field gradient as it is, in principle, fully tunable. We define the layer bias $h = xW + h_0$ as a fraction x of the bandwidth of the intralayer dispersion $W = \max \varepsilon_{\mathbf{k}} - \min \varepsilon_{\mathbf{k}}$ with an additional offset h_0 to shift the dispersion to have $\tilde{\varepsilon}_{\mathbf{0}} = 0$. We show in Fig. 5 how this allows control over the unstable manifolds, from a single point at $k_c = (0, 0)$ for $x = 0$ (left top panel) over ringlike structures around the center of the Brillouin zone at intermediate x (central top panel) to arcs around the corners of the Brillouin zone (BZ) as x approaches 1 (top right panel).

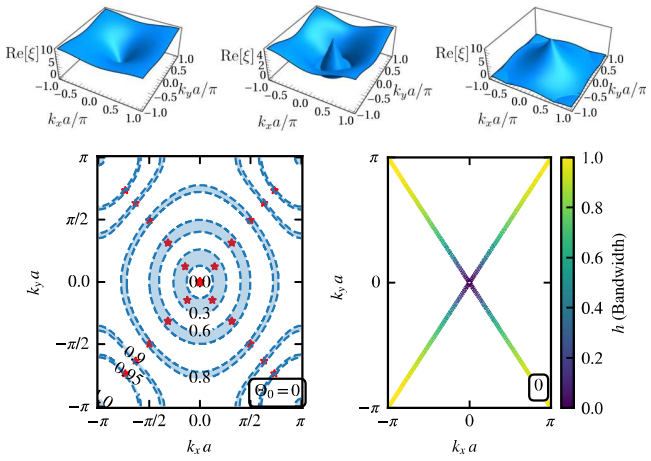

FIG. 5. Tunability of unstable modes via electric field gradient at $\Theta_0 = 0$. Top panel: Real part of the Bogoliubov quasienergy $\xi_{\mathbf{k}}$ in units of $J/\hbar$ at $\Theta_0 = 0.0$ and $a_Z/a = 2$ for different applied field gradients $x = 0, 0.5, 0.95$, from left to right. The applied field gradient is defined via a fraction x of the total bandwidth $W = \max \varepsilon_{\mathbf{k}} - \min \varepsilon_{\mathbf{k}}$ as $h = xW + h_0$, where h_0 is chosen to shift the dispersion to have $\tilde{\varepsilon}_{\mathbf{0}} = 0$. Bottom left panel: Manifolds of unstable modes defined as the nonvanishing imaginary part of the Bogoliubov energy $\xi_{\mathbf{k}}$. Red stars indicate the most unstable mode. Bottom right panel: Contours of the most unstable mode $\mathbf{k}_*$ as a function of the applied field gradient (color bar).

The instabilities are pushed to the four corners of the BZ at $x = 1$. This is shown more directly in the right bottom panel of Fig. 5, which shows the behavior of the most unstable mode as a function of the layer bias.

We note that for $\Theta_0 = 0$, the most unstable mode is always fourfold degenerate for $\Theta_0 = 0$, with the exception of the case of $k \to 0$ and close to the degenerate region along rings around the center of the BZ. In contrast, for other dipole orientations, e.g., $\Theta_0 = \pi/4$ (not shown), the most unstable mode may be either twofold or fourfold degenerate and of the form $\mathbf{k}_* = \pm\mathbf{k}$ or $\mathbf{k}_* = (\pm k_x, \pm k_y)$. In addition, we observe another distinct topology of unstable modes consisting of two separate disklike regions.

V. FULL SPIN DYNAMICS

We next turn to the full quantum spin dynamics of the model obtained within the DTWA [50,51]. The momentum state population of excitations in layer B maps to the structure factor, which in terms of spin operators can be written as

$$\hat{N}^B_{\mathbf{k}} = \frac{1}{N}\sum_{\mathbf{ij}} e^{i\mathbf{k}\cdot(\mathbf{r_i}-\mathbf{r_j})}\hat{b}^\dagger_{\mathbf{i}}\hat{b}_{\mathbf{j}} = \frac{1}{N}\sum_{\mathbf{ij}} e^{i\mathbf{k}\cdot(\mathbf{r_i}-\mathbf{r_j})}\hat{s}^+_{\mathbf{i}}\hat{s}^-_{\mathbf{j}}, \qquad (4)$$

with a similar expression for layer A and we define $N_{\mathbf{k}} = \langle\hat{N}^A_{\mathbf{k}}\rangle = \langle\hat{N}^B_{\mathbf{k}}\rangle$. Note that the disconnected part vanishes identically (see the Appendix). We will focus on this momentum structure to observe the pair creation process in the spin dynamics (see the Appendix for real-space results).

Figure 1(b) shows the population $N_{k^*}(t)$ of the most unstable mode k^* for different dipole orientations Θ_0 obtained from both DTWA simulations (solid lines) and the Bogoliubov analysis (dashed lines) with no fitting parameters. Both results are in very good agreement in the initial exponential growth regime (regime I), in which a significant number of pairs are created before corrections or further scattering terms become important. This is followed in the full dynamics by a slow down and eventual saturation to a maximal mode occupation (regime II), after which scattering between momentum modes starts to deplete the maximally unstable mode (regime III). As expected from the Bogoliubov analysis, we observe that the spatial and temporal growth of correlations exhibit a strong dependence on the dipole orientation.

We show the time evolution of the full momentum distribution of the created pairs during the spin dynamics of the model, obtained within DTWA for a representative $\Theta_0 = 3\pi/8$ in Fig. 6(a), with an extended set of figures provided in the Appendix. At very short times, off-resonant non-exponentially-growing modes dominate the structure (left panel), which then give way to the exponentially growing unstable modes resulting in the distribution expected from the Bogoliubov prediction (second panel). Naturally, higher-order terms neglected within the Bogoliubov approximation will eventually result in scattering between different momentum modes, leading to thermalization. This expectation is seen in the last two panels showing first an increase of population in the slower growing unstable modes and then thermalization in the late-time regime. We note that the approach to equilibrium can itself host rich physics [52–55].

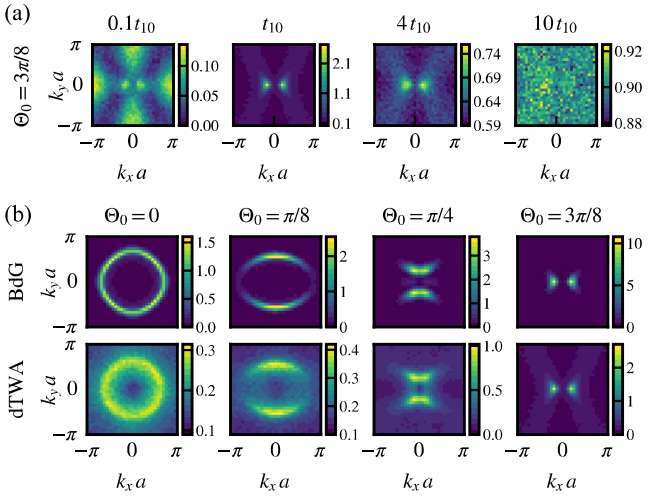

FIG. 6. Momentum structure of created pairs $N_{\mathbf{k}}$. (a) Time evolution of $N_{\mathbf{k}}(t)$ within DTWA showing the different regimes of dynamics for $\Theta_0 = 3\pi/8$. Time in terms of t_{10}, where $N_{\text{pair}}(t_{10}) = 0.1N$. The leftmost panel shows the early-time regime before exponential growth has taken over. The second panel shows the buildup of the expected momentum structure. The last two panels show the subsequent thermalization as scattering between momentum modes occurs. (b) Comparison of Bogoliubov prediction (top) and spin dynamics from DTWA (bottom) for a range of Θ_0, all at t_{10}. Results are for a 33×33 bilayer with layer spacing $a_Z/a = 2$ with open-boundary conditions at unit filling.

We establish the correspondence of the DTWA results and the Bogoliubov predictions for different dipole orientations Θ_0 in Fig. 6(b). Here, we choose an evolution time t such that the total number of pairs $N_{\text{pair}} = \sum_{\mathbf{k}} N_{\mathbf{k}}(t) = 0.1N$, to allow time for the dynamical instability to create pairs, while at the same time keeping within the regime of validity of the Bogoliubov analysis. We observe good agreement for all dipole orientations, indicating that the pair production mechanism is still effective in the full dipolar spin model.

VI. WIDER CONTEXT

After establishing these phenomena in the full spin dynamics, we can now connect back to the motivating ideas. Conceptually, we realize quantum-time evolution of the form $|\psi(t)\rangle \simeq e^{\Gamma t \sum_{\mathbf{k}\in\eta_c} \beta_{\mathbf{k}}^\dagger \beta_{\mathbf{k}}} |\text{vac}\rangle$, where $|\text{vac}\rangle$ is the vacuum of excitations, η_c is the set of most unstable momentum modes, and $\beta_{\mathbf{k}}$ are the quasiparticle operators. This generates pairs of correlated excitations with opposite momenta in the layers; the momentum distribution at momentum $\mathbf{k}$ in layer A equals that at momentum $-\mathbf{k}$ in layer B, which reflects the strongly entangled character of the state generated during pair creation.

As a direct consequence of realizing a pair-creation Hamiltonian of momentum modes, the quantum dynamics maps onto Unruh radiation [34]: the created population of excitations in momentum space is exactly the thermal bath observed in an accelerated frame (see the Appendix). Moreover, the time-evolved state (see the Appendix) is the thermofield double state [35,36], which, within the the holographic correspondence, is dual to wormholes on the gravity side [56,57]

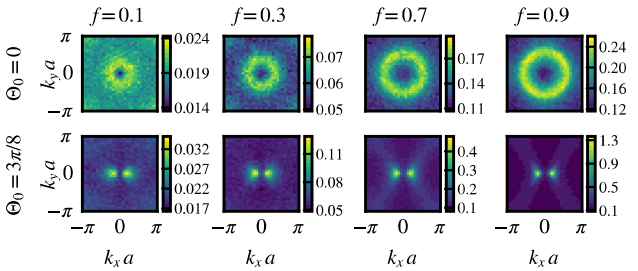

FIG. 7. Momentum occupation $N_{\mathbf{k}}$ of created pairs in the presence of positional disorder and nonunit filling obtained within DTWA. Results are for a range of Θ_0 and filling fraction f at fixed $a_Z/a = 2$ at times such that $N_{\text{pair}}(t) = 0.1fN$. $L = 33$ with open-boundary conditions.

and enables teleportation ("traversable wormholes") [37–39]. It is also an ideal resource for EPR steering [25–28] given its shared entanglement between spatially separated layers. Finally, the entangled pairs in the form of a two-mode squeezed state [29] also feature correlations in the amplitude and phase quadratures of the momentum modes: their individual fluctuations are amplified, while their relative fluctuations are reduced below the vacuum noise level, enabling applications in quantum metrology.

VII. IMPERFECT FILLING

Considering the feasibility to observe these effects in an experimental setting, while tweezer arrays offer the possibility to achieve unit filling [20–23,58–60], a major challenge in optical lattices, especially for polar molecules, is imposed by imperfect filling, which results in positional disorder of the pinned dipoles. While important developments in cooling and trapping molecules have allowed the preparation of lattice arrays with up to $f = 0.25$ [18,61–63], which highlight the near-future potential of achieving high filling fractions, they also illustrate the need to understand which effects would be observable at lower filling fractions in current setups.

To address this question, we consider bilayers in which each lattice site has a fixed spatially uniform probability f to be occupied or empty. We show the resulting momentum occupation N_k for different filling fractions f (averaging over 10 000 filling realizations) and two dipole orientations Θ_0 in Fig. 7. Also, for the case of imperfect filling, our DTWA results are in very good agreement with the Bogoliubov analysis (for more details, see the Appendix). We observe that while the signal to noise deteriorates as the lattice becomes more sparsely filled, most importantly, the main qualitative phenomenology, i.e., the emergence of a manifold of unstable exponentially growing modes, does extend to a remarkably low filling fraction regime, which makes the observation in experimental platforms feasible.

VIII. OUTLOOK

Dipolar systems confined in two-dimensional bilayers host a dynamical instability generating correlated pairs and entanglement between spatially separated layers. Making use

of the wide tunability of dipolar interactions, one can access different shapes and topologies of the momentum distribution of the created pairs. These correlations may be probed using spatially resolved measurements accessible in state-of-the-art platforms in tweezers and quantum gas microscopes for a range of atomic or molecular gases. In these systems, the entangled pairs in spatially separated layers can be stored and manipulated with individual particle control, providing new opportunities in metrology.

The reported dynamical instabilities not only are genuinely driven by quantum fluctuations, but are in stark contrast to the usual rotonlike instabilities at finite momentum, as, e.g., in dipolar condensates [64]; here the generated modes of opposite momentum $\pm\vec{k}$ are not equivalent, but rather correspond to two different entangled pairs of excitations in both layers.

The long-time behavior and eventual thermalization of the excitations remain an open question. Since the initial pairing instability creates a well-defined highly nonthermal occupation in momentum space, the eventual approach to equilibrium might reveal universal nonequilibrium scaling exponents and self-similarity [52–55].

ACKNOWLEDGMENTS

We acknowledge careful review of this manuscript and useful comments from A. Carroll and J. Higgins. G.A.D.-C. and L.S. acknowledge support of the Deutsche Forschungsgemeinschaft (DFG, German Research Foundation) under Germany's Excellence Strategy – EXC-2123 QuantumFrontiers – Grant No. 390837967. D.W. and A.M.R. acknowledge support from the AFOSR MURI, the ARO single investigator Award No. W911NF-19-1-0210, the NSF JILA-PFC PHY-1734006 grants, and the NSF QLCI-2016244 grants, by the US Department of Energy Quantum Systems Accelerator (QSA) grant and by NIST.

APPENDIX

The appendices contain additional details on the Bogoliubov analysis, the effect of boundary conditions, the real-space structure of the spin correlations, and Bogoliubov as well as extended DTWA results for the finite filling fraction behavior of the momentum structure of correlations, and extended DTWA results for the time dependence.

1. Bogoliubov analysis

Here we provide further details of the Bogoliubov analysis of the spin Hamiltonian. First, we focus on the diagonalization procedure of a unit filling lattice, then we proceed to discuss the case of lattices with fillings smaller than one. For a perfectly filled lattice, we may write the Hamiltonian in quasimomentum space,

$$\hat{H} = \sum_{\mathbf{k}} \varepsilon_{\mathbf{k}} (\hat{a}^\dagger_{\mathbf{k}} \hat{a}_{\mathbf{k}} + \hat{b}^\dagger_{\mathbf{k}} \hat{b}_{\mathbf{k}}) + \sum_{\mathbf{k}} |[\Omega_{\mathbf{k}}| e^{-i\alpha_{\mathbf{k}}} \hat{a}^\dagger_{\mathbf{k}} \hat{b}^\dagger_{-\mathbf{k}} + |\Omega_{\mathbf{k}}| e^{i\alpha_{\mathbf{k}}} \hat{a}_{\mathbf{k}} \hat{b}_{-\mathbf{k}}], \tag{A1}$$

where we have made explicit the complex nature of the interlayer coupling $\Omega_{\mathbf{k}} = |\Omega_{\mathbf{k}}| e^{-i\alpha_{\mathbf{k}}}$. In the presence of an Ising term, we would simply substitute $\varepsilon_{\mathbf{k}}$ by $\tilde{\varepsilon}_{\mathbf{k}}$. Before introducing the Bogoliubov transformation, it is convenient to decouple the above Hamiltonian into symmetric and antisymmetric collective quasimomentum modes. For this purpose, we define the following operators:

$$\hat{S}_{\mathbf{k}} = \frac{1}{\sqrt{2}} (e^{-i\alpha_{\mathbf{k}}/2} \hat{a}_{\mathbf{k}} + e^{i\alpha_{\mathbf{k}}/2} \hat{b}_{\mathbf{k}}),$$
$$\hat{A}_{\mathbf{k}} = \frac{1}{\sqrt{2}} (e^{-i\alpha_{\mathbf{k}}/2} \hat{a}_{\mathbf{k}} - e^{i\alpha_{\mathbf{k}}} \hat{b}_{\mathbf{k}}). \tag{A2}$$

In terms of these new operators, the Hamiltonian can be rewritten as $\hat{H} = \hat{H}_S + \hat{H}_A$ with

$$\hat{H}_S = \sum_{\mathbf{k}} \varepsilon_{\mathbf{k}} \hat{S}^\dagger_{\mathbf{k}} \hat{S}_{\mathbf{k}} + \frac{|\Omega_{\mathbf{k}}|}{2} (\hat{S}^\dagger_{\mathbf{k}} \hat{S}^\dagger_{-\mathbf{k}} + \hat{S}_{\mathbf{k}} \hat{S}_{-\mathbf{k}}),$$
$$\hat{H}_A = \sum_{\mathbf{k}} \varepsilon_{\mathbf{k}} \hat{A}^\dagger_{\mathbf{k}} \hat{A}_{\mathbf{k}} - \frac{|\Omega_{\mathbf{k}}|}{2} (\hat{A}^\dagger_{\mathbf{k}} \hat{A}^\dagger_{-\mathbf{k}} + \hat{A}_{\mathbf{k}} \hat{A}_{-\mathbf{k}}). \tag{A3}$$

In the following, we discuss the diagonalization of $\hat{H}_S$, but that of $\hat{H}_A$ is completely analogous. At this point, we introduce the Bogoliubov transformation $\hat{\beta}_{\mathbf{k}} = u_{\mathbf{k}} \hat{S}_{\mathbf{k}} - v^*_{\mathbf{k}} \hat{S}^\dagger_{-\mathbf{k}}$. The amplitudes $u_{\mathbf{k}}$ and $v_{\mathbf{k}}$ obey the Bogoliubov–de Gennes equations,

$$\xi_{\mathbf{k}} u_{\mathbf{k}} = \varepsilon_{\mathbf{k}} u_{\mathbf{k}} + |\Omega_{\mathbf{k}}| v_{\mathbf{k}}, \tag{A4}$$

$$\xi_{\mathbf{k}} v_{\mathbf{k}} = -|\Omega_{\mathbf{k}}| u_{\mathbf{k}} - \varepsilon_{\mathbf{k}} v_{\mathbf{k}}, \tag{A5}$$

where the eigenenergies acquire the form $\xi_{\mathbf{k}} = \sqrt{\varepsilon^2_{\mathbf{k}} - |\Omega_{\mathbf{k}}|^2}$. In the case of real eigenvalues, the time dependence of the Bogoliubov operators is $\hat{\beta}_{\mathbf{k}}(t) = e^{-i\xi_{\mathbf{k}} t} \hat{\beta}_{\mathbf{k}}(0)$ and $\hat{\beta}^\dagger_{\mathbf{k}}(t) = e^{i\xi_{\mathbf{k}} t} \hat{\beta}^\dagger_{\mathbf{k}}(0)$. Inversion of the Bogoliubov transformation yields the following expression:

$$\hat{S}_{\mathbf{k}}(t) = [e^{-i\xi_{\mathbf{k}} t} \cosh^2 \phi_{\mathbf{k}} - e^{i\xi_{\mathbf{k}} t} \sinh^2 \phi_{\mathbf{k}}] \hat{S}_{\mathbf{k}}(0) + i \sinh(2\phi_{\mathbf{k}}) \sin(\xi_{\mathbf{k}} t) \hat{S}^\dagger_{\mathbf{k}}(0), \tag{A6}$$

with $\sinh^2 2\phi_{\mathbf{k}} = |\Omega_{\mathbf{k}}|^2 / \xi^2_{\mathbf{k}}$. The vacuum expectation value of the population of the symmetric mode $\mathbf{k}$ gives $\langle 0|\hat{S}^\dagger_{\mathbf{k}}(t) \hat{S}_{\mathbf{k}}(t)|0\rangle = \sinh^2(2\phi_{\mathbf{k}}) \sin^2(\xi_{\mathbf{k}} t)$; the same expression fulfills $\langle 0|\hat{A}^\dagger_{\mathbf{k}}(t) \hat{A}_{\mathbf{k}}(t)|0\rangle$. Then, the total population of the mode is simple,

$$N_{\mathbf{k}} = \langle \hat{A}^\dagger_{\mathbf{k}}(t) \hat{A}_{\mathbf{k}}(t) + \hat{S}^\dagger_{\mathbf{k}}(t) \hat{S}_{\mathbf{k}}(t) \rangle / 2 = [|\Omega_{\mathbf{k}}| \sin(\xi_{\mathbf{k}} t) / \xi_{\mathbf{k}}]^2. \tag{A7}$$

If $\xi_{\mathbf{k}}$ is imaginary, the Bogoliubov modes fulfill $|u_{\mathbf{k}}|^2 = |v_{\mathbf{k}}|^2$ and therefore the modes are actually quadratures of the form

$$\hat{X}_{\mathbf{k}} = \frac{1}{\sqrt{\sin \phi_{\mathbf{k}}}} [e^{-i\phi_{\mathbf{k}}/2} \hat{S}_{\mathbf{k}} - e^{i\phi_{\mathbf{k}}/2} \hat{S}^\dagger_{-\mathbf{k}}],$$
$$\hat{P}_{\mathbf{k}} = \frac{1}{\sqrt{\sin \phi_{\mathbf{k}}}} [e^{i\phi_{\mathbf{k}}/2} \hat{S}_{\mathbf{k}} - e^{-i\phi_{\mathbf{k}}/2} \hat{S}^\dagger_{-\mathbf{k}}], \tag{A8}$$

with $\tan \phi_{\mathbf{k}} = -\varepsilon_{\mathbf{k}} / |\xi_{\mathbf{k}}|$. The first quadrature grows exponentially in time, $\hat{X}_{\mathbf{k}}(t) = e^{|\xi_{\mathbf{k}}| t} \hat{X}_{\mathbf{k}}(0)$, whereas $\hat{P}_{\mathbf{k}}(t) = e^{-|\xi_{\mathbf{k}}| t} \hat{P}_{\mathbf{k}}(0)$ decreases exponentially. By inverting the definition of the quadratures, one can find the time evolution of the symmetric mode,

$$\hat{S}_{\mathbf{k}} = \frac{i}{\sqrt{2 \sin \phi_{\mathbf{k}}}} [(e^{-i\phi_{\mathbf{k}}} e^{|\xi_{\mathbf{k}}| t} - e^{i\phi_{\mathbf{k}}} e^{-|\xi_{\mathbf{k}}| t}) \hat{S}_{\mathbf{k}}(0) - 2 \sinh(|\xi_{\mathbf{k}}| t) \hat{S}^\dagger_{-\mathbf{k}}(0)]. \tag{A9}$$

Then it follows that $\langle \hat{S}^{\dagger}_{\mathbf{k}}(t)\hat{S}_{\mathbf{k}}(t)\rangle = \sinh^2(|\xi_{\mathbf{k}}|t)/\sin^2\phi^2_{\mathbf{k}}$; a similar expression fulfills $\langle \hat{A}^{\dagger}_{\mathbf{k}}(t)\hat{A}_{\mathbf{k}}(t)\rangle$. The total population of the mode is simple, $N_{\mathbf{k}} = [|\Omega_{\mathbf{k}}|\sinh(|\xi_{\mathbf{k}}|t)/|\xi_{\mathbf{k}}|]^2$. Since $\sin(i|\xi_{\mathbf{k}}|)/i|\xi_{\mathbf{k}}| \to -\sinh(|\xi_{\mathbf{k}}|)/|\xi_{\mathbf{k}}|$, one can safely use the expression in Eq. (A7) to obtain the time dependence of the density of excitations in each layer,

$$n(t)a^2 = \int_{\mathrm{BZ}} \frac{d^2k}{(2\pi)^2}|\Omega_k|^2\left[\frac{\sin|\xi_{\mathbf{k}}|t}{|\xi_{\mathbf{k}}|}\right], \tag{A10}$$

where the integration is over the first Brillouin zone.

The Bogoliubov treatment of the case of imperfect filling is more involved. We consider a lattice with $L \times L$ sites with open-boundary conditions, and a filling $f < 1$. We create a given realization by randomly filling each layer with a given number of dipoles, up to the desired lattice filling. Due to positional disorder, it is suitable to work with the Hamiltonian in space representation,

$$\hat{H} = \sum_{\mathbf{i}\neq\mathbf{j}} V^{AA}_{\mathbf{ij}}\hat{a}^{\dagger}_{\mathbf{i}}\hat{a}_{\mathbf{j}} + \sum_{\mathbf{i}\neq\mathbf{j}} V^{BB}_{\mathbf{ij}}\hat{b}^{\dagger}_{\mathbf{i}}\hat{b}_{\mathbf{j}} + \sum_{\mathbf{i},\mathbf{j}} V^{AB}_{\mathbf{ij}}\hat{a}^{\dagger}_{\mathbf{i}}\hat{b}^{\dagger}_{\mathbf{j}} + \sum_{\mathbf{i},\mathbf{j}} V^{BA}_{\mathbf{ij}}\hat{b}_{\mathbf{i}}\hat{a}_{\mathbf{j}}. \tag{A11}$$

We may again apply the Bogoliubov transformation, $\hat{\beta}_n = \sum_{\mathbf{j}} u_{n\mathbf{j}}\hat{a}_{\mathbf{j}} + \sum_{\mathbf{j}'} v_{n\mathbf{j}'}\hat{b}_{\mathbf{j}'}$. By imposing that $\xi_n\hat{\beta}_n = [\hat{\beta}_n, \hat{H}]$, we obtain the Bogoliubov–de Gennes equations,

$$\xi_n\begin{pmatrix}\mathbf{u}_n\\ \mathbf{v}_n\end{pmatrix} = \begin{pmatrix}V^{AA} & -V^{AB}\\ V^{BA} & -V^{BB}\end{pmatrix}\begin{pmatrix}\mathbf{u}_n\\ \mathbf{v}_n\end{pmatrix}, \tag{A12}$$

where $\mathbf{u}_n = (u_{n,\mathbf{i}_1}, u_{n,\mathbf{i}_2}\ldots u_{n,\mathbf{i}_{L\times L}})^T$ and similarly for $\mathbf{v}_n$. By solving the above eigenvalue problem, we obtain the eigenmodes and their corresponding evolution in time. Inverting the Bogoliubov transformation provides the time dependence of the lattice operators, and Fourier transforming yields the quasimomentum distribution. Averaging over many random realizations of the lattice filling, we obtain the distributions discussed below.

2. Pair creation for quantum simulation and metrology

Here we provide additional details of the relevance of the discussed pair-creation mechanism to quantum simulation and metrology.

At the center of these connections is that we effectively realize pair creation at resonant momenta, or a two-mode squeezing Hamiltonian involving momentum modes. This allows for the generation of the so-called thermofield double (TFD) states. TFD states are not only at the heart of quantum simulation of Unruh radiation [34], but also a resource for entanglement generation between spatially separated modes which can be used for various applications ranging from quantum metrology to teleportation and quantum communication.

To make these connections as transparent as possible, we restrict, for simplicity, to a single resonant mode, for which we effectively realize

$$h_{\mathbf{k}_c} = (\Omega_{\mathbf{k}_c}\hat{a}^{\dagger}_{\mathbf{k}_c}\hat{b}^{\dagger}_{-\mathbf{k}_c} + \Omega^{*}_{\mathbf{k}_c}\hat{a}_{-\mathbf{k}_c}\hat{b}_{\mathbf{k}_c}), \tag{A13}$$

which is the well-known two-mode squeezing Hamiltonian, which here creates entangled pairs in spatially separated layers A and B.

The operators consequently evolve as

$$\begin{pmatrix}\hat{a}_k(t)\\ \hat{b}^{\dagger}_{-k}(t)\end{pmatrix} = \begin{pmatrix}\cosh(|\Omega_{\mathbf{k}_c}|t/\hbar) & \sinh(|\Omega_{\mathbf{k}_c}|t/\hbar)\\ \sinh(|\Omega_{\mathbf{k}_c}|t/\hbar) & \cosh(|\Omega_{\mathbf{k}_c}|t/\hbar)\end{pmatrix}\begin{pmatrix}\hat{a}_k(0)\\ \hat{b}^{\dagger}_{-k}(0)\end{pmatrix}. \tag{A14}$$

One can compare this directly to the transformation into the Rindler frame of a scalar field [34], which is given by

$$\begin{pmatrix}\hat{b}^{R}_{\omega}\\ \hat{b}^{\dagger L}_{\omega}\end{pmatrix} = \begin{pmatrix}\cosh(r_\omega) & \sinh(r_\omega)\\ \sinh(r_\omega) & \cosh(r_\omega)\end{pmatrix}\begin{pmatrix}\hat{c}_{\omega}\\ \hat{d}^{\dagger}_{\omega}\end{pmatrix}, \tag{A15}$$

where $\tanh(r_\omega) = e^{-\pi\omega c/a}$ is defined in terms of the acceleration a of the frame and the frequency ω of the field. This connects field operators in an accelerated frame on the left, to Unruh operators on the right whose vacuum is the Minkowski vacuum in the inertial frame.

An evolution time t for a given resonant mode $\mathbf{k}_c$ then corresponds to a frame transformation with acceleration

$$a = -\pi\omega c/\ln[\tanh(|\Omega_{\mathbf{k}_c}|t/\hbar)], \tag{A16}$$

and the excitations created in the quantum system during the time evolution thus correspond to the thermal occupation of modes observed in an accelerated frame, i.e., a process that quantum simulates Unruh radiation.

If we now take a closer look at the generated state after time evolution, which emerges from the vacuum state, it has the form

$$e^{ith_{\mathbf{k}_c}}|\mathrm{vac}\rangle = \frac{1}{\cosh(|\Omega_{\mathbf{k}_c}|t)}\sum_{n=0}^{\infty}\tanh^n(|\Omega_{\mathbf{k}_c}|t)|n_{A,\mathbf{k}_c}, n_{B,-\mathbf{k}_c}\rangle, \tag{A17}$$

which is known in the literature as a thermofield double state (TFD) [35–37]. This is a pure state of the form

$$\frac{1}{\sqrt{Z}}\sum_n e^{-En/(2k_bT)}|n\rangle_A \otimes |n\rangle_B, \tag{A18}$$

where the coefficients follow a Boltzmann distribution with a temperature set by the evolution time as

$$T = \frac{E}{2k_B\ln[\coth(|\Omega_{\mathbf{k}_c}|t)]}. \tag{A19}$$

The Boltzmann-like distribution generated in a pure quantum state has the appeal that when each of the modes of the TFD is considered independently by tracing over the other,

$$\rho_{\mathrm{reduced}} = \frac{1}{Z}\sum_n e^{-En/(k_bT)}|n\rangle\langle n|, \tag{A20}$$

the state reduces to a thermal mixed state with an effective temperature T [35]. These types of states have played a key role in the holographic correspondence relating a quantum-field theory to a gravitational theory in one higher dimension. In this correspondence, TFD states are dual to wormholes on the gravity side [56,57] and enable teleportation ("transversable wormholes") [38,39].

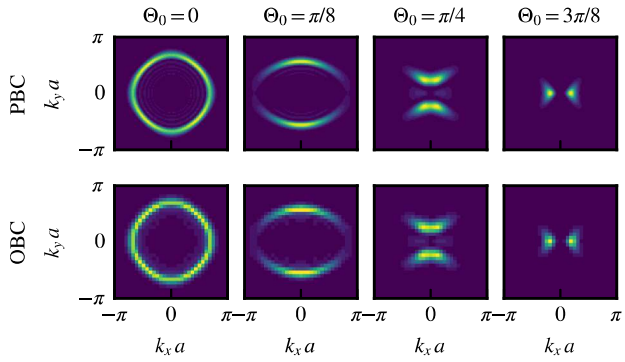

FIG. 8. Effect of the boundary conditions in the Bogoliubov analysis. We depict the quasimomentum distribution of the created pairs, N_k, comparing periodic (top) and open (bottom) boundary conditions for a range of dipole orientations Θ_0, at times such that $N_{\text{pair}}(t) = \sum_{\mathbf{k}} N_{\mathbf{k}}(t) = 0.1N$. The results were obtained for a 33×33 bilayer with layer spacing $a_Z/a = 2$ at unit filling.

3. Comparison of open and closed boundary conditions

The above-mentioned procedure in real space for $f < 1$ may also be employed for full filling, providing the time evolution in the presence of open-boundary conditions, rather than periodic boundary conditions, as implicitly assumed in the analysis in quasimomentum space. We consider the effects of boundary conditions on the momentum structure of the created pairs in finite systems within the Bogoliubov analysis in Fig. 8. We see that both periodic (top) and open (bottom) boundaries result in basically the same momentum structure across all dipole orientations. This demonstrates that the predicted phenomena should be accessible within the limitations of total particle numbers and lattice sizes available in experimental platforms.

4. Comparison of momentum and real-space structure of correlations

Here we provide results for the correlation structure in real space. While we mainly focus on the momentum structure of the correlations, as they directly map to the occupation of momentum modes and the Bogoliubov analysis, the real-space correlations are what would be directly observed in an experiment with access to spatially resolved measurements.

By defining the spin-spin correlation function

$$C^{+-}_{\mathbf{ij}} = \langle \hat{s}^+_{\mathbf{i}} \hat{s}^-_{\mathbf{j}} \rangle, \tag{A21}$$

the spin-structure factor $S^{A(B),+-}_{\mathbf{k}}$, which corresponds to the momentum mode occupation in the low excitation limit, is just

$$S^{A(B),+-}_{\mathbf{k}} = \frac{1}{N} \sum_{\mathbf{ij} \in A(B)} e^{i\mathbf{k}(\mathbf{r_i} - \mathbf{r_j})} C^{+-}_{\mathbf{ij}}. \tag{A22}$$

We emphasize that this directly corresponds to the connected correlation function for our initial state evolving under the U(1)-symmetric *XXZ* Hamiltonian which makes the one-point functions vanish identically at all times, i.e., $\langle \hat{s}^+_i \rangle = \langle \hat{s}^-_i \rangle = 0$.

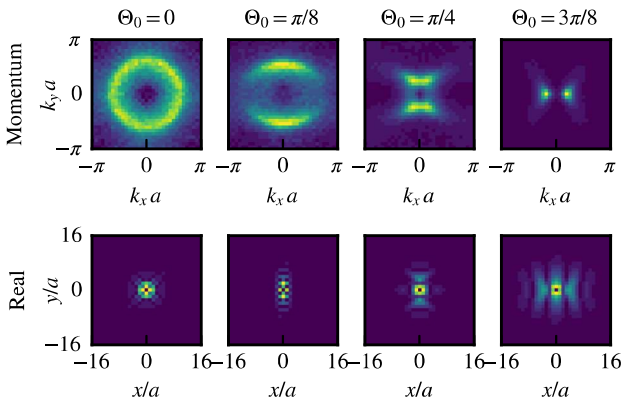

FIG. 9. Correlations in momentum and real space. Top panel: Spin-structure factor $S^{+-}_{\mathbf{k}}(t)$ [see Eq. (A22)], corresponding to momentum state population of pairs $N_k(t)$, compared to the real-space structure of spin correlations $|C^{+-}_{\mathbf{r}}(t)|$ [see Eq. (A21)]. Results are for a 33×33 bilayer with a layer spacing of $a_Z/a = 2$ and open-boundary conditions at time t such that $N_{\text{pair}}(t) = N/10$.

We compare these expressions directly in Fig. 9 for a range of dipole orientations. The top panels show the spin-structure factor $S^{+-}_{\mathbf{k}}$, and the bottom panels show the corresponding real-space correlation function $C^{+-}_{\mathbf{r}}$ at a distance $\mathbf{r} = \mathbf{r_i} - \mathbf{r_j}$, both summed over the layers A, B. To make the structure of real-space correlations visible on top of the population growth, we only show them for $\mathbf{i} \neq \mathbf{j}$, e.g., set $C^{+-}_{\mathbf{ii}} = 0$. These results highlight the intricate real-space structure of the correlations created during the pair-creation process. We note that up to boundary effects, the density of excitations itself is fully homogeneous throughout the dynamics, and the structure emerges within the intersite off-diagonal correlations.

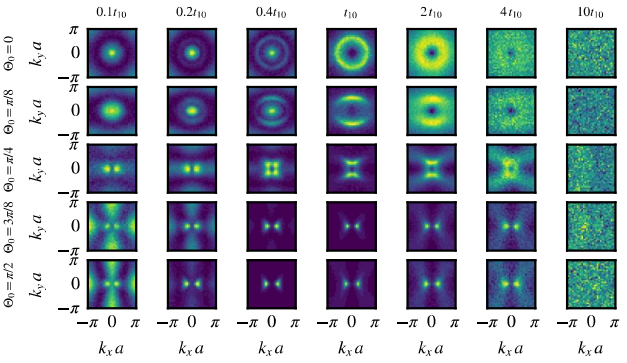

FIG. 10. Extended DTWA results on time evolution. Momentum state population of pairs $N_k(t)$ within DTWA showing the different regimes of dynamics for a range of dipole orientations Θ_0 at times in terms of t_{10} at which $N_{\text{pair}}(t_{10}) = 0.1N$. The leftmost panel shows the early-time regime before exponential growth has taken over. The second and third panels show the buildup of the expected momentum structure. The central panel shows the fully builtup expected momentum structure. The last three panels show the subsequent thermalization as scattering between momentum modes occurs. Results are for a 33×33 bilayer with a layer spacing of $a_Z/a = 2$ and open-boundary conditions.

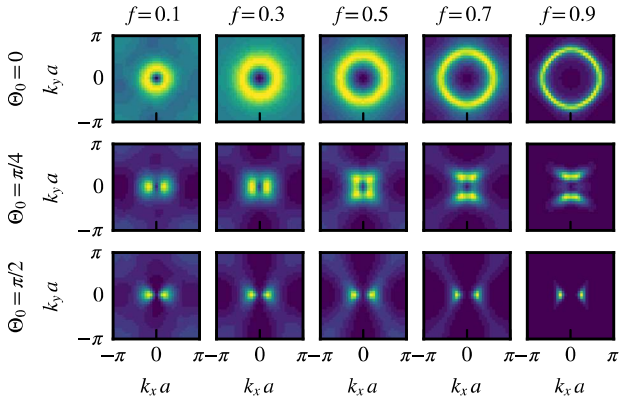

FIG. 11. Bogoliubov results at finite filling. Momentum state population N_k for a range of Θ_0 and filling fraction f at times such that $N_{\mathrm{pair}}(t) = 0.1fN$. Results are for a 33×33 bilayer with a layer spacing of $a_Z/a = 2$ and open-boundary conditions.

5. Extended results on time dependence

We provide extended results for the time dependence of the momentum structure of the created pairs obtained within DTWA in Fig. 10. This provides both the full range of dipole orientations (in contrast to the single case of $\Theta_0 = 3\pi/8$ in the main text), as well as additional times during the buildup of correlations, as well as during the late-time thermalization state. The qualitative picture remains the same for all dipole orientations, in that at very early times, the dynamics of stable modes can dominate over the exponentially growing unstable modes, which establish the expected momentum structure at intermediate times, before scattering between modes leads to thermalization and a homogeneous background at late times.

6. Results at finite filling

Figure 11 shows the quasimomentum distribution of the created pairs for an imperfect filling within the Bogoliubov analysis, following the procedure discussed above. These results should be compared with the results shown in Fig. 3(b) of the main text, as well as with the results covering an expanded set of dipole orientations in Fig. 12. The DTWA results are averaged over 10 000 realizations of the lattice occupations, whereas the Bogoliubov results average over 200 realizations.

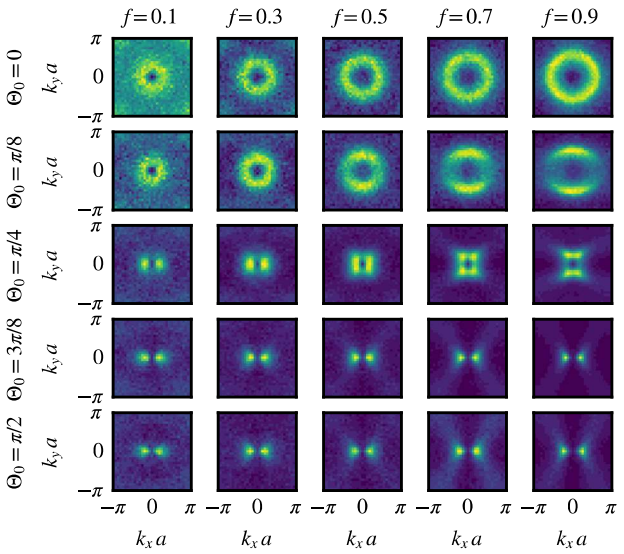

FIG. 12. Extended DTWA results at finite filling. Momentum structure of created pairs $N_{\mathbf{k}}(t)$ at times t such that the total number of pairs $N_{\mathrm{pair}}(t) = 0.1fN$. Results are for a range of Θ_0 and filling fraction f for a 33×33 bilayer with a layer spacing of $a_Z/a = 2$ and open-boundary conditions.

Across all dipole orientations and filling fractions, we again observe a very good agreement between the spin dynamics obtained with the DTWA and the Bogoliubov predictions. In particular, both show the shrinking of the structures in momentum space as the filling fraction is lowered. Intuitively, large momentum modes would be expected to be more strongly affected by the introduction of local disorder, whereas small momentum modes would be expected to be more resilient, which seems to be the case here.

Importantly, the dynamics remains qualitatively unaffected by the imperfect filling, being still characterized by the exponential growth of characteristic patterns in quasimomentum space, that depend on the dipole orientation. This robustness against imperfect filling is particularly relevant since it makes feasible the observation of the effect in current experimental platforms.

[1] M. A. Baranov, M. Dalmonte, G. Pupillo, and P. Zoller, Condensed matter theory of dipolar quantum gases, Chem. Rev. **112**, 5012 (2012).

[2] J. L. Bohn, A. M. Rey, and J. Ye, Cold molecules: Progress in quantum engineering of chemistry and quantum matter, Science **357**, 1002 (2017).

[3] S. A. Moses, J. P. Covey, M. T. Miecnikowski, D. S. Jin, and J. Ye, New frontiers for quantum gases of polar molecules, Nat. Phys. **13**, 13 (2017).

[4] L. Chomaz, I. Ferrier-Barbut, F. Ferlaino, B. Laburthe-Tolra, B. L. Lev, and T. Pfau, Dipolar physics: A review of experiments with magnetic quantum gases, Rep. Prog. Phys. **86**, 026401 (2023).

[5] A. Browaeys and T. Lahaye, Many-body physics with individually controlled Rydberg atoms, Nat. Phys. **16**, 132 (2020).

[6] M. Saffman, T. G. Walker, and K. Mølmer, Quantum information with Rydberg atoms, Rev. Mod. Phys. **82**, 2313 (2010).

[7] S. de Léséleuc, V. Lienhard, P. Scholl, D. Barredo, S. Weber, N. Lang, H. P. Büchler, T. Lahaye, and A. Browaeys, Observation of a symmetry-protected topological phase of interacting bosons with Rydberg atoms, Science **365**, 775 (2019).

[8] B. Yan, S. A. Moses, B. Gadway, J. P. Covey, K. R. A. Hazzard, A. M. Rey, D. S. Jin, and J. Ye, Observation of dipolar spin-exchange interactions with lattice-confined polar molecules, Nature (London) **501**, 521 (2013).

[9] A. de Paz, A. Sharma, A. Chotia, E. Maréchal, J. H. Huckans, P. Pedri, L. Santos, O. Gorceix, L. Vernac, and B. Laburthe-Tolra, Nonequilibrium Quantum Magnetism in a Dipolar Lattice Gas, Phys. Rev. Lett. **111**, 185305 (2013).

[10] K. R. A. Hazzard, B. Gadway, M. Foss-Feig, B. Yan, S. A. Moses, J. P. Covey, N. Y. Yao, M. D. Lukin, J. Ye, D. S. Jin, and A. M. Rey, Many-Body Dynamics of Dipolar Molecules in an Optical Lattice, Phys. Rev. Lett. **113**, 195302 (2014).

[11] S. Lepoutre, J. Schachenmayer, L. Gabardos, B. Zhu, B. Naylor, E. Maréchal, O. Gorceix, A. M. Rey, L. Vernac, and B. Laburthe-Tolra, Out-of-equilibrium quantum magnetism and thermalization in a spin-3 many-body dipolar lattice system, Nat. Commun. **10**, 1714 (2019).

[12] L. Gabardos, B. Zhu, S. Lepoutre, A. M. Rey, B. Laburthe-Tolra, and L. Vernac, Relaxation of the Collective Magnetization of a Dense 3d Array of Interacting Dipolar $s = 3$ atoms, Phys. Rev. Lett. **125**, 143401 (2020).

[13] A. Patscheider, B. Zhu, L. Chomaz, D. Petter, S. Baier, A.-M. Rey, F. Ferlaino, and M. J. Mark, Controlling dipolar exchange interactions in a dense three-dimensional array of large-spin fermions, Phys. Rev. Res. **2**, 023050 (2020).

[14] T. Bilitewski, L. De Marco, J.-R. Li, K. Matsuda, W. G. Tobias, G. Valtolina, J. Ye, and A. M. Rey, Dynamical Generation of Spin Squeezing in Ultracold Dipolar Molecules, Phys. Rev. Lett. **126**, 113401 (2021).

[15] W. G. Tobias, K. Matsuda, J.-R. Li, C. Miller, A. N. Carroll, T. Bilitewski, A. M. Rey, and J. Ye, Reactions between layer-resolved molecules mediated by dipolar spin exchange, Science **375**, 1299 (2022).

[16] T. Bilitewski and A. M. Rey, Manipulating growth and propagation of correlations in dipolar multilayers: From pair production to bosonic Kitaev models, arXiv:2211.12521.

[17] J.-R. Li, K. Matsuda, C. Miller, A. N. Carroll, W. G. Tobias, J. S. Higgins, and J. Ye, Tunable itinerant spin dynamics with polar molecules, Nature (London) **614**, 70 (2023).

[18] L. Christakis, J. S. Rosenberg, R. Raj, S. Chi, A. Morningstar, D. A. Huse, Z. Z. Yan, and W. S. Bakr, Probing site-resolved correlations in a spin system of ultracold molecules, Nature (London) **614**, 64 (2023).

[19] C. Gross and W. S. Bakr, Quantum gas microscopy for single atom and spin detection, Nat. Phys. **17**, 1316 (2021).

[20] A. M. Kaufman and K.-K. Ni, Quantum science with optical tweezer arrays of ultracold atoms and molecules, Nat. Phys. **17**, 1324 (2021).

[21] C. M. Holland, Y. Lu, and L. W. Cheuk, On-demand entanglement of molecules in a reconfigurable optical tweezer array, arXiv:2210.06309.

[22] Y. Bao, S. S. Yu, L. Anderegg, E. Chae, W. Ketterle, K.-K. Ni, and J. M. Doyle, Dipolar spin-exchange and entanglement between molecules in an optical tweezer array, arXiv:2211.09780.

[23] L. Anderegg, L. W. Cheuk, Y. Bao, S. Burchesky, W. Ketterle, K.-K. Ni, and J. M. Doyle, An optical tweezer array of ultracold molecules, Science **365**, 1156 (2019).

[24] J. T. Zhang, Y. Yu, W. B. Cairncross, K. Wang, L. R. B. Picard, J. D. Hood, Y.-W. Lin, J. M. Hutson, and K.-K. Ni, Forming a Single Molecule by Magnetoassociation in an Optical Tweezer, Phys. Rev. Lett. **124**, 253401 (2020).

[25] A. Einstein, B. Podolsky, and N. Rosen, Can quantum-mechanical description of physical reality be considered complete? Phys. Rev. **47**, 777 (1935).

[26] M. D. Reid, P. D. Drummond, W. P. Bowen, E. G. Cavalcanti, P. K. Lam, H. A. Bachor, U. L. Andersen, and G. Leuchs, Colloquium: The Einstein-Podolsky-Rosen paradox: From concepts to applications, Rev. Mod. Phys. **81**, 1727 (2009).

[27] M. Fadel, T. Zibold, B. Décamps, and P. Treutlein, Spatial entanglement patterns and Einstein-Podolsky-Rosen steering in Bose-Einstein condensates, Science **360**, 409 (2018).

[28] P. Kunkel, M. Prüfer, H. Strobel, D. Linnemann, A. Frölian, T. Gasenzer, M. Gärttner, and M. K. Oberthaler, Spatially distributed multipartite entanglement enables EPR steering of atomic clouds, Science **360**, 413 (2018).

[29] G. Agarwal, *Quantum Optics* (Cambridge University Press, Cambridge, 2013).

[30] J. Schwinger, On gauge invariance and vacuum polarization, Phys. Rev. **82**, 664 (1951).

[31] P. Hauke, D. Marcos, M. Dalmonte, and P. Zoller, Quantum Simulation of a Lattice Schwinger Model in a Chain of Trapped Ions, Phys. Rev. X **3**, 041018 (2013).

[32] V. Kasper, F. Hebenstreit, M. Oberthaler, and J. Berges, Schwinger pair production with ultracold atoms, Phys. Lett. B **760**, 742 (2016).

[33] W. G. Unruh, Notes on black-hole evaporation, Phys. Rev. D **14**, 870 (1976).

[34] J. Hu, L. Feng, Z. Zhang, and C. Chin, Quantum simulation of Unruh radiation, Nat. Phys. **15**, 785 (2019).

[35] Y. Takahashi and H. Umezawa, Thermo field dynamics, Intl. J. Mod. Phys. B **10**, 1755 (1996).

[36] S. Chapman, J. Eisert, L. Hackl, M. P. Heller, R. Jefferson, H. Marrochio, and R. C. Myers, Complexity and entanglement for thermofield double states, SciPost Phys. **6**, 034 (2019).

[37] D. Zhu, S. Johri, N. M. Linke, K. A. Landsman, C. H. Alderete, N. H. Nguyen, A. Y. Matsuura, T. H. Hsieh, and C. Monroe, Generation of thermofield double states and critical ground states with a quantum computer, Proc. Natl. Acad. Sci. USA **117**, 25402 (2020).

[38] P. Gao, D. L. Jafferis, and A. C. Wall, Traversable wormholes via a double trace deformation, J. High Energy Phys. 12 (2017) 151.

[39] J. Maldacena, D. Stanford, and Z. Yang, Diving into traversable wormholes, Fortschr. Phys. **65**, 1700034 (2017).

[40] C. Gross, H. Strobel, E. Nicklas, T. Zibold, N. Bar-Gill, G. Kurizki, and M. K. Oberthaler, Atomic homodyne detection of continuous-variable entangled twin-atom states, Nature (London) **480**, 219 (2011).

[41] B. Lücke, M. Scherer, J. Kruse, L. Pezzé, F. Deuretzbacher, P. Hyllus, O. Topic, J. Peise, W. Ertmer, J. Arlt, L. Santos, A. Smerzi, and C. Klempt, Twin matter waves for interferometry beyond the classical limit, Science **334**, 773 (2011).

[42] A. Sørensen, L.-M. Duan, J. I. Cirac, and P. Zoller, Many-particle entanglement with Bose-Einstein condensates, Nature (London) **409**, 63 (2001).

[43] A. Qu, B. Evrard, J. Dalibard, and F. Gerbier, Probing Spin Correlations in a Bose-Einstein Condensate Near the Single-Atom Level, Phys. Rev. Lett. **125**, 033401 (2020).

[44] C. Klempt, O. Topic, G. Gebreyesus, M. Scherer, T. Henninger, P. Hyllus, W. Ertmer, L. Santos, and J. J. Arlt, Multiresonant Spinor Dynamics in a Bose-Einstein Condensate, Phys. Rev. Lett. **103**, 195302 (2009).

[45] B. Sundar, D. Barberena, A. P. Orioli, A. Chu, J. K. Thompson, A. M. Rey, and R. J. Lewis-Swan, Bosonic Pair Production and Squeezing for Optical Phase Measurements in Long-Lived Dipoles Coupled to a Cavity, Phys. Rev. Lett. **130**, 113202 (2023).

[46] A. Periwal, E. S. Cooper, P. Kunkel, J. F. Wienand, E. J. Davis, and M. Schleier-Smith, Programmable interactions and emergent geometry in an array of atom clouds, Nature (London) **600**, 630 (2021).

[47] J. Nipper, J. B. Balewski, A. T. Krupp, S. Hofferberth, R. Löw, and T. Pfau, Atomic Pair-State Interferometer: Controlling and Measuring an Interaction-Induced Phase Shift in Rydberg-Atom Pairs, Phys. Rev. X **2**, 031011 (2012).

[48] M. L. Wall, K. R. A. Hazzard, and A. M. Rey, Quantum magnetism with ultracold molecules, in *From Atomic to Mesoscale*, edited by S. Malinovskaya and I. Novikova (World Scientific, Singapore, 2015), pp. 3–37.

[49] C. Chen, G. Bornet, M. Bintz, G. Emperauger, L. Leclerc, V. S. Liu, P. Scholl, D. Barredo, J. Hauschild, S. Chatterjee, M. Schuler, A. M. Läuchli, M. P. Zaletel, T. Lahaye, N. Y. Yao, and A. Browaeys, Continuous symmetry breaking in a two-dimensional Rydberg array, Nature **616**, 691 (2023).

[50] J. Schachenmayer, A. Pikovski, and A. M. Rey, Many-Body Quantum Spin Dynamics with Monte Carlo Trajectories on a Discrete Phase Space, Phys. Rev. X **5**, 011022 (2015).

[51] B. Zhu, A. M. Rey, and J. Schachenmayer, A generalized phase space approach for solving quantum spin dynamics, New J. Phys. **21**, 082001 (2019).

[52] M. Prüfer, P. Kunkel, H. Strobel, S. Lannig, D. Linnemann, C.-M. Schmied, J. Berges, T. Gasenzer, and M. K. Oberthaler, Observation of universal dynamics in a spinor Bose gas far from equilibrium, Nature (London) **563**, 217 (2018).

[53] S. Erne, R. Bücker, T. Gasenzer, J. Berges, and J. Schmiedmayer, Universal dynamics in an isolated one-dimensional Bose gas far from equilibrium, Nature (London) **563**, 225 (2018).

[54] J. A. P. Glidden, C. Eigen, L. H. Dogra, T. A. Hilker, R. P. Smith, and Z. Hadzibabic, Bidirectional dynamic scaling in an isolated Bose gas far from equilibrium, Nat. Phys. **17**, 457 (2021).

[55] J. F. Rodriguez-Nieva, A. P. Orioli, and J. Marino, Far-from-equilibrium universality in the two-dimensional Heisenberg model, Proc. Natl. Acad. Sci. **119**, e2122599119 (2022).

[56] W. Israel, Thermofield dynamics of black holes, Phys. Lett. A **57**, 107 (1976).

[57] J. Maldacena, Eternal black holes in anti–de Sitter, J. High Energy Phys. 04 (2003) 021.

[58] M. Endres, H. Bernien, A. Keesling, H. Levine, E. R. Anschuetz, A. Krajenbrink, C. Senko, V. Vuletic, M. Greiner, and M. D. Lukin, Atom-by-atom assembly of defect-free one-dimensional cold atom arrays, Science **354**, 1024 (2016).

[59] D. Barredo, S. de Léséleuc, V. Lienhard, T. Lahaye, and A. Browaeys, An atom-by-atom assembler of defect-free arbitrary two-dimensional atomic arrays, Science **354**, 1021 (2016).

[60] J. T. Zhang, L. R. B. Picard, W. B. Cairncross, K. Wang, Y. Yu, F. Fang, and K.-K. Ni, An optical tweezer array of ground-state polar molecules, Quantum Sci. Technol. **7**, 035006 (2022).

[61] L. De Marco, G. Valtolina, K. Matsuda, W. G. Tobias, J. P. Covey, and J. Ye, A degenerate Fermi gas of polar molecules, Science **363**, 853 (2019).

[62] G. Valtolina, K. Matsuda, W. G. Tobias, J.-R. Li, L. D. Marco, and J. Ye, Dipolar evaporation of reactive molecules to below the fermi temperature, Nature (London) **588**, 239 (2020).

[63] S. A. Moses, J. P. Covey, M. T. Miecnikowski, B. Yan, B. Gadway, J. Ye, and D. S. Jin, Creation of a low-entropy quantum gas of polar molecules in an optical lattice, Science **350**, 659 (2015).

[64] L. Chomaz, R. M. W. van Bijnen, D. Petter, G. Faraoni, S. Baier, J. H. Becher, M. J. Mark, F. Wächtler, L. Santos, and F. Ferlaino, Observation of roton mode population in a dipolar quantum gas, Nat. Phys. **14**, 442 (2018).